Material Properties Imaging of Cross-Linked Polymers by NMR

W. Kuhn,* P. Barth, and S. Hafner†

Fraunhofer-Institut für Biomedizinische Technik, Ensheimer Strasse 48, D-66386 St. Ingbert, Federal Republic of Germany

G. Simon‡ and H. Schneider

Fachbereich Physik, Martin-Luther Universität Halle, Friedemann-Bach-Platz 6, D-06108 Halle (Saale), Federal Republic of Germany

Received February 18, 1994; Revised Manuscript Received June 24, 1994®

ABSTRACT: Spatially resolved investigations of molecular properties in polymer materials are shown to be possible by means of parameter-selective NMR imaging. The transformation of NMR parameters into material properties can be performed using a suitable theoretical description of the molecular mobility in the polymer under investigation. Rubber samples consisting of three pieces of rubber with different cross-link densities have been investigated in a first experiment. A series of images which were progressively weighted by transverse relaxation have been acquired by application of a spin–echo back-projection technique. The relaxation was analyzed pixel by pixel using a single chain model for the molecular dynamics of the polymer network. Parameters directly related to material parameters, such as cross-link density and correlation times, could be derived from the theory and were displayed in the form of a MAterial Property image (MAP image). In contrast to conventional spin density images, where the different pieces of rubber could not be distinguished properly, the MAP image clearly reflects the different cross-link densities. Moreover, histogram analysis of the image can be used for the characterization of cross-link density inhomogeneities.

Introduction

The application of NMR imaging to rubber materials is quite recent. First papers[1–5] show that ^{1}H-NMR imaging can be used to investigate the morphology of semirigid materials with an in-plane resolution of about 100 μm. Compared to other imaging techniques such as light or electron microscopy, the achievable spatial resolution in NMR imaging is quite poor for many physical and technical reasons. This disadvantage, however, is compensated for by two important advantages. NMR imaging is a nondestructive subsurface technique, and it gives access to spatially resolved spectroscopic and parameter-selective information.

Parameter-selective NMR imaging, especially NMR relaxation time imaging, has become valuable for the investigation of polymer materials. Depending on the applied magnetization filter preceding the imaging sequence, the relaxation times of the nuclear magnetization, T_1, $T_{1\rho}$, or T_2, can be determined for each voxel from a series of relaxation time weighted images and displayed as a parameter-selective image. Since NMR relaxation is related to the molecular structure and mobility, such images reflect these properties. In ref 6 several authors present spatially resolved investigations of aging, stretching, and swelling of materials using this technique.

Materials scientists, however, are interested not so much in images of NMR typical parameters like relaxation times but much more in images of material properties. As a first step, a strain image has been obtained using the T_2–strain relationship, which was determined experimentally for the investigated sample prior to the imaging experiment.[7] The aim of this work is to extend NMR imaging to a technique, which allows one to reveal material parameters directly by means of a suitable theoretical analysis of the NMR data. Interpretation of data taken from an image has been performed earlier[8] on swollen samples using the Bloembergen–Purcell–Pound (BPP) expression. In this paper we will show for the first time images of material parameters, which were derived by analysis of transverse NMR relaxation taking into account the nonexponentiality of the transverse decay in unswollen polymer networks. It is just this nonexponentiality, which is not accounted for in conventional T_2 images, that contains the information on the properties of the polymer material such as cross-link density and molecular mobility of the chains. In order to relate the measured NMR relaxation data to the properties of the investigated polymer material, a theoretical model is required, which describes the chain dyanmics in cross-linked polymers.

Theory

Transverse ^{1}H-NMR relaxation is caused by inter- and intramolecular dipolar interaction of protons. In polymer networks at temperatures above the glass transition temperature, this interaction is averaged by the thermal molecular motion. The interpretation of transverse NMR relaxation, which we will use in the following, is based on a modified single-chain model where the protons of the hydrocarbon chain are taken as probes for the NMR measurement. This model was successfully tested earlier[9–12] and has been described in full detail in ref. 13. Hence, we would like to discuss only the main features here. The theory is based on the following assumptions:

(1) The network consists of inter-cross-link chains and dangling chain ends with different molecular mobility. Consequently, the corresponding transverse relaxation signals are different in shape and time behavior.

(2) Real chains are replaced by noninteracting Kuhn chains[14] consisting of free jointed statistical segments with protons which interact along the segment axis.

(3) Inter-cross-link chains are fixed at both ends. The motional statistics provides a mean, small anisotropy of the fast local motion (correlation time τ_f on the order of 10^{-9} s) of the Kuhn statistical segments.[14] Consequently, a small part of the dipolar interaction is left and expressed as the ratio q of the remaining second moment and the second moment M_2 of the rigid lattice.

† Present address: Max-Planck-Institut für Polymerforschung, Postfach 3148, D-55021 Mainz, Germany.

‡ Present address: Varian GmbH, Alsfelder Strasse 3, D-64289 Darmstadt, Germany.

® Abstract published in *Advance ACS Abstracts*, August 15, 1994.

0024-9297/94/2227-5773$04.50/0

(4) The remaining dipolar interaction can only be diminished by an overall isotropic motion of the whole inter-cross-link chain. As a result of the larger size of the moving object, the correlation time τ_s of this motion is on the order of 10^{-3} s.

(5) Dangling chain ends are fixed only on one side. Therefore, the segmental motion, which is characterized by the same correlation time τ_f as the fast motion of the inter-cross-link chains, is isotropic ($q = 0$). Consequently, the dipolar interaction is already averaged out by this process, and the overall isotropic motion with the correlation time τ_s does not have any effect on the relaxation function.

For rubber networks, the range of molecular dynamics is intermediate between the motional narrowing and the rigid lattice case. The transverse relaxation $M(t)$ for correlation times τ_c much greater than the Larmor period ($\omega_0\tau_c \gg 1$) is well described by the Anderson–Weiss formula.[15]

$$M(t) = M(0)\exp\{-\int_0^t G(\tau)\,(t-\tau)\,d\tau\} \quad (1)$$

Assuming a simple exponential correlation function $G(\tau) = M_2\exp(-\tau/\tau_c)$, the transverse relaxation $M(t)$ is given by

$$M(t) = M(0)\exp\{-M_2\tau_c^2[\exp(-t/\tau_c) + t/\tau_c - 1]\} \quad (2)$$

If the correlation time is much shorter than the observation time ($\tau_c \ll t$ (decay time)), the BPP formula[16,17] is valid, again assuming a simple exponential correlation function:

$$\frac{1}{T_2(\tau_c)} = M_2\tau_c\left[1 + \frac{5/3}{1+\omega_0^2\tau_c^2} + \frac{2/3}{1+4\omega_0^2\tau_c^2}\right] \quad (3)$$

and a single-exponential decay appears: $M(t) \sim \exp(-t/T_2(\tau_c))$. The intermediate case, if both conditions are fulfilled, follows by use of (2) and (3): $M(t) \sim \exp(-tM_2\tau_c)$.

Taking into account assumptions 1–5, appropriate correlation functions can be derived[9,13] relating the molecular dynamics with NMR relaxation parameters. For inter-cross-link chains this correlation function is given by

$$G(\tau) = [(1-q)M_2\exp(-\tau/\tau_f) + qM_2]\exp(-\tau/\tau_s) \quad (4)$$

and can be approximated for $q \ll 1$ and $\tau_f \ll \tau_s$ by

$$G(\tau) \approx M_2\exp(-\tau/\tau_f) + qM_2\exp(-\tau/\tau_s) \quad (5)$$

This leads to a Gauss-like relaxation function. The relaxation function for the dangling chain ends is a pure exponential function since $q = 0$. The total transverse magnetization function is composed of both contributions and is given by[9,13]

$$M(t) = A\exp\left\{\frac{-t}{T_2(\tau_f)} - qM_2\tau_s^2\left[\exp\left(\frac{-t}{\tau_s}\right) + \frac{t}{\tau_s} - 1\right]\right\} + B\exp\left(\frac{-t}{T_2(\tau_f)}\right) \quad (6)$$

A and B are the fractions of magnetization (equivalent to the mass fractions) of the inter-cross-link chains and the dangling chain ends of the network, respectively.

From the theoretical point of view, the residual "static" dipolar interaction qM_2 is pure intramolecular. At temperatures far above the glass transition temperature, intermolecular magnetic interactions can be neglected.[13] Consequently, M_2 in (2)–(6) will be the intramolecular part of the second moment of the rigid lattice. It can be determined at temperatures below the glass transition temperature from the transverse relaxation in samples which are swollen with a hydrogen-free solvent (e.g., CCl_4). The relaxation follows a Gaussian or Abragam decay function[16] providing M_2 directly.

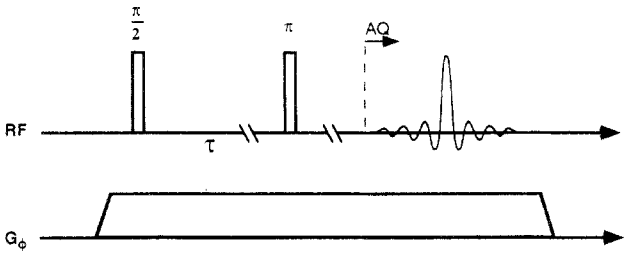

Figure 1. Pulse sequence used for material imaging experiments. It consists of a conventional spin-echo back-projection sequence with variation of the spin-echo time 2τ.

The factor *1* of the second moment was shown to be a sum of contributions of the physical (q_0) and chemical cross-links (q').[10–13] The contribution q_0 can be determined experimentally using the same procedure for a sample without chemical cross-links. The factor q', which corresponds to the contribution of the chemical cross-links, can be evaluated for the model as described above and, as a confirmation, also for the more realistic tube model with strong restrictions.[18] Both approaches give nearly the same q' value[19] of $q' = (3/(5N))^2 - k$, where N is the number of the Kuhn statistical segments in the inter-cross-link chain and k is an additional correction factor of the tube model, which contains the tube diameter and the length of the statistical segment. In our case, it is on the order of some percent of q' and will be neglected. The factor q' is related to the molecular mass M_c of the chain between chemical cross-links by[9–13,19]

$$M_c = \frac{3cM_{ru}}{5n\sqrt{q'}} \quad (7)$$

where c is the number of backbone bonds in a Kuhn segment and M_{ru}/n represents the mass of the chemical repeating units per number of backbone bonds. Assuming a cross-link functionality of 4, the cross-link density is $v_c = \rho/2M_c$, whre ρ is the mass density. From eq 7 follows the proportionality of q' to the square of v_c.

Experimental Section

The validity of the theory was already shown[10–13] by conventional measurements of the transverse relaxation times in rubber samples with well-known cross-link densities. The measurement of the transverse decay of the magnetization has been performed using a Hahn spin-echo sequence with variation of the spin-echo time to eliminate the influence of magnetic field inhomogeneities and of the chemical shift on the transverse decay, while the dipolar interaction is not affected. Equation 6 was fitted to the experimental data, and the material parameters were calculated from the fit results.

This method can easily be extended to an imaging experiment. Figure 1 shows the pulse program used for the spatially resolved measurements. It consists of a Hahn spin-echo back-projection sequence, with the gradients applied during the whole sequence. The spin-echo time 2τ is stepped, and the echo is acquired for each step. The echo decay contains the image information, while the decay due to the transverse relaxation is encoded in the form of the echo amplitudes.

The relaxation weighted images were reconstructed from these data sets using a homemade implementation of the back-projection algorithm.[20] From this series of images the magnetization decay can be calculated for each voxel. In order to achieve a convergent fit under all circumstances, eq 6 has been ap-

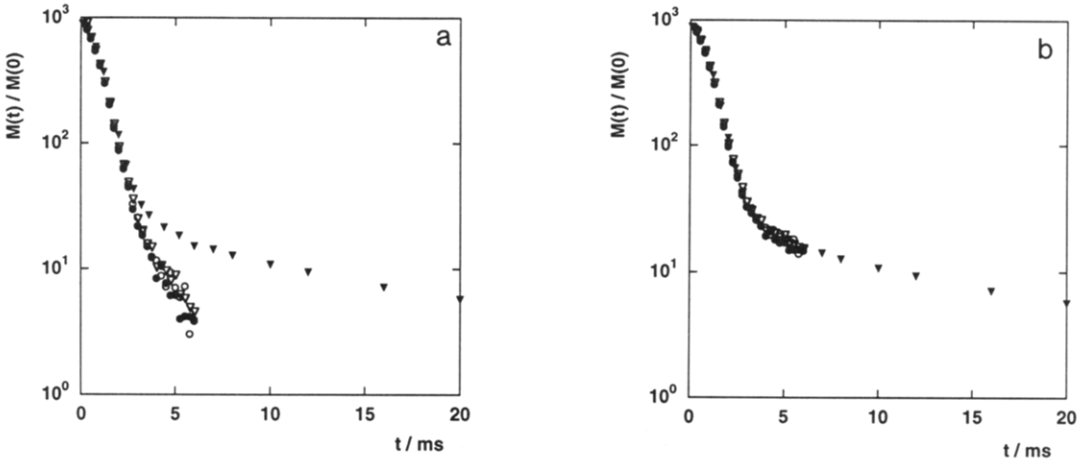

Figure 2. (a) Comparison of the transverse relaxation for a bulk measurement (▼) and for three arbitrarily selected voxels from an image (other symbols), taken for a piece of rubber with a cross-link density of 6.6×10^{-5} mol/cm^3. The data correspond very well to each other for short spin-echo times. The deviations for long time values are due to the sensitivity of the back-projection procedure to small errors in the profiles. (b) Same decay as in part a after zero level correction by addition of a constant value of about 1% of the amplitude. The decays taken from the bulk measurement and the data from the imaging experiments correspond well to each other for the entire time range.

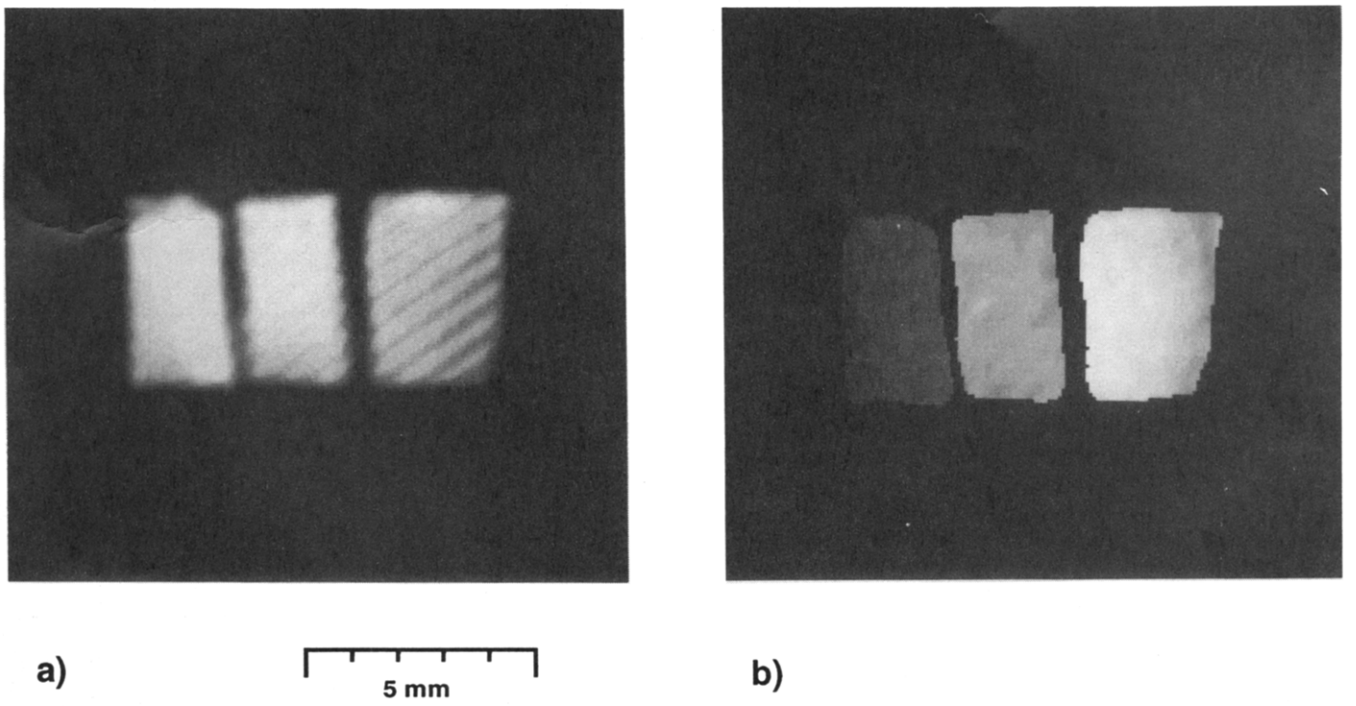

Figure 3. (a) Conventional spin density image of a sample consisting of three pieces of rubber with different cross-link densities (without filler). The cross-link density is increasing from left to right (v_c values: 3.8×10^{-5}, 6.6×10^{-5}, and 9.8×10^{-5} mol/cm^3). The different cross-link densities cannot be distinguished in this image. (b) Material parameter image with respect to qM_2. This parameter is proportional to the square of the cross-link density. In this "cross-link density" image the different cross-link densities of the three rubber pieces can easily be distinguished.

proximated by

$$M(t) = A \exp\left(\frac{-t}{T_2} - \frac{qM_2t^2}{2}\right) + B \exp\left(\frac{-t}{T_2}\right) \qquad (8)$$

which is allowed for $\tau_s \gg t$ (decay time) and is approximately fulfilled in our case ($\tau_s \geq t$). The fit parameters are the fractions of the inter-cross-link chains (A) and the dangling chain ends (B), the fraction of the second moment qM_2, which is related to the cross-link density, and T_2, which is given approximately by $T_2 = 1/(M_2\tau_f)$. The fit has been performed using the Marquardt–Levenberg algorithm, and the resulting parameters for all voxels are displayed as an image using the SUNRISE software environment.[21] The reliability of the fit procedure was tested in earlier publications.[10-13] Using different sets of starting parameters, the fit always converged to the same results, which were in good accordance with other, independent measurements.

The measurements were carried out on a Varian Unity-400 spectrometer equipped for microimaging. A Varian Broad-band probe, whose B_1 characteristics were optimized in our radio frequency laboratory by a homemade 5-mm solenoidal coil insert, was used. The 90° pulse length was 1.5 μs. The echo time 2τ was varied between 300 μs and 6 ms in 24 steps. A gradient of 35 G/cm was stepped by 128 angle increments for the back-projection procedure. The pixel resolution of the 256×256 pixel image was 70×70 μm. For reasons of better signal-to-noise no slice selection was applied. The spatial resolution in the third direction therefore was 1.3 mm, the thickness of the sample. The experiments were performed using a pulse repetition time of 3 s (approximately 4 times T_1) so that the measurement time of the full set of images was about 10 h (four averages).

Two test samples were investigated. The first sample was composed of three pieces of unfilled natural rubber with different

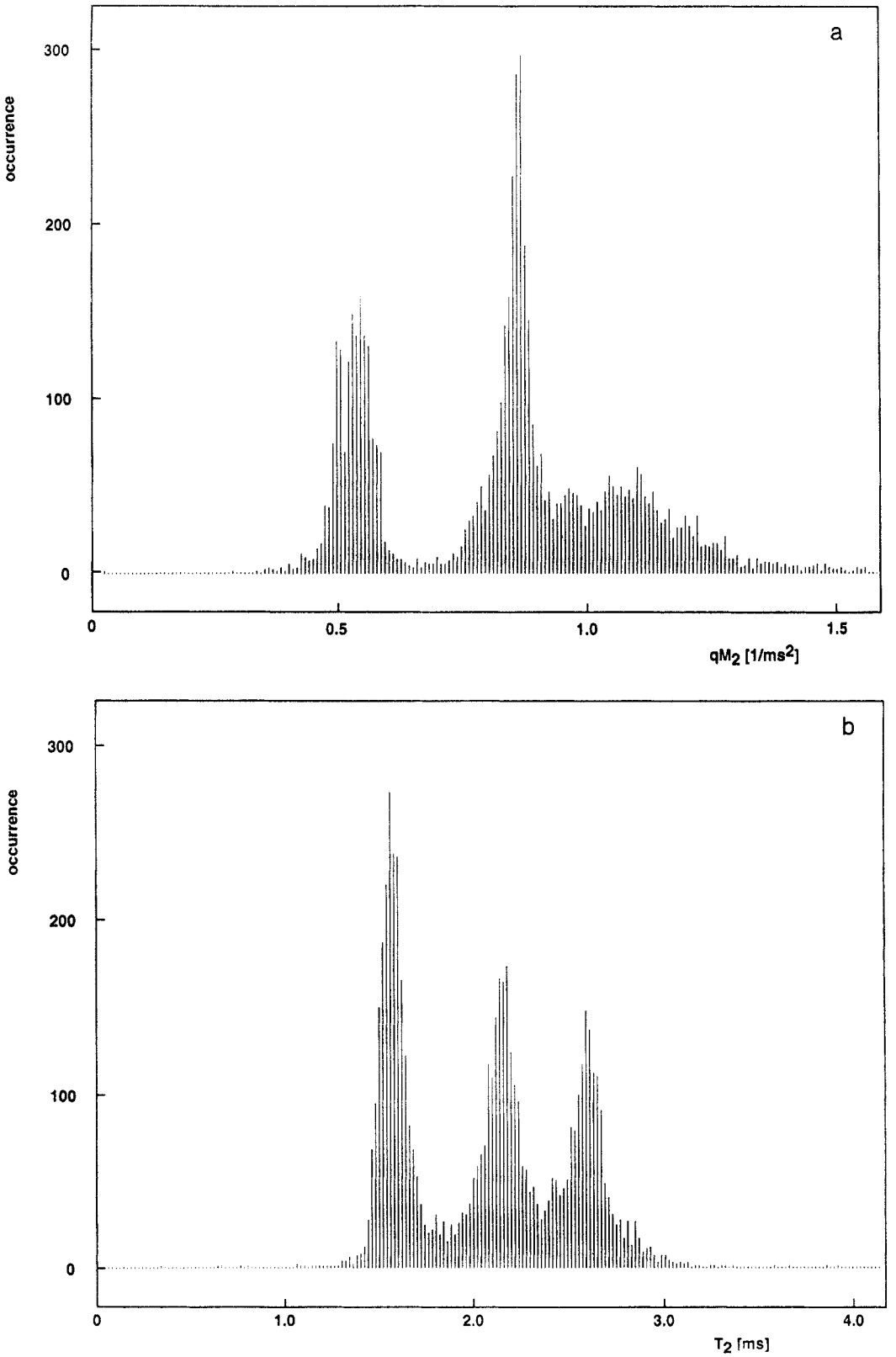

Figure 4. (a) Histogram analysis of the qM_2 distribution (corresponding to the cross-link density distribution) within the whole sample. The three maxima, which are well separated from each other, correspond to the center values of each of the pieces. The width of the three peaks is a measure of the qM_2 or cross-link density distribution, respectively, within the single rubber pieces. (b) Histogram analysis of the T_2 distribution (the sample with the highest cross-link density is on the left-hand side). From theoretical point of view, this parameter is not so sensitive to changes in the cross-link density. If the corrected relaxation values could be displayed, the variation in the T_2 values would be much smaller.

cross-link densities (v_c values: 3.8×10^{-5}, 6.6×10^{-5}, and 9.8×10^{-5} mol/cm^3). The second sample consisted also of three pieces of rubber, for which the same amount of cross-linking agent was used as for the corresponding pieces of the first sample but which are filled with carbon black (≈20 vol %). The raw material was standardized malaysian rubber, which was mixed with 3 phr (parts per hundred rubber) zinc oxide, with 1 phr stearic acid, and with an increasing amount (0.8 phr, 1.6 phr, 2.4 phr) of a 1:1 sulfur–*N*-cyclohexylbenzthiazol-2-sulfenamide. The material was pressed to plates of about 10 cm × 10 cm × 1.3 mm and had been cured at 155 °C at 14 min. The rubber pieces used for the investigations were cut from the middle part of the plates.

Knowing from previous relaxation measurements on the whole sample that the sol content is very small (very long exponential

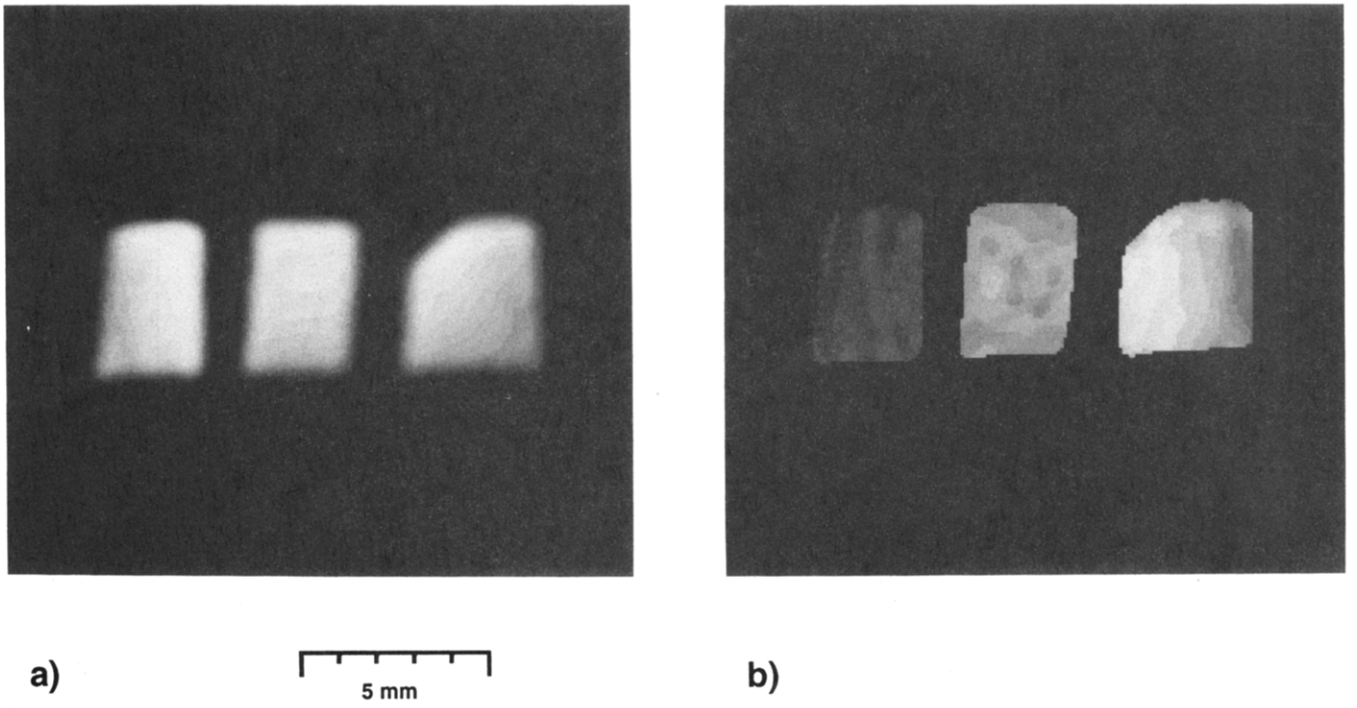

Figure 5. (a) Spin density image of a sample consisting of three pieces of filled rubber. The cross-link densities of the three pieces of rubber are about the same as in the sample without filler (compare Figure 3a). (b) Calculated qM_2 image of the sample with filler, corresponding to an image of the cross-link density of the sample. The result is approximately the same for the sample without filler.

tail of less than 1% as a third component), the sol component was not extracted.

Results and Discussion

Figure 2a shows a comparison of the experimental data from a bulk measurement of the rubber material, corresponding to the piece in the middle of sample 1, with the data of three arbitrarily selected pixels from the image given in Figure 3. The data of the three pixels correspond excellently to each other and, for short spin-echo times, also to the data from the bulk measurement. The deviations on the long time scale are due to a zero level problem of up to 1% of the maximum value resulting from the instability of the back-projection procedure to small artifacts in the profiles. This discrepancy can be corrected for by a zero level correction for the spatially resolved measurements. Figure 2b shows the transverse decay after this correction. The values are in good accordance with each other. Unfortunately, the zero level is not constant over the whole image, so this correction factor must basically be determined for each pixel with the procedure described above. For this reason, no correction was performed for the evaluation of the images.

Figure 3 shows a conventional spin density image of the first sample with $2\tau = 300$ μs. As expected, the different cross-link densities of the three rubber pieces cannot be distinguished in this image.

Figure 3b shows a qM_2 image of the sample, corresponding to an image of the square of the cross-link density. The three pieces of rubber are easily discriminated by their different qM_2 values. The structures within the single rubber pieces are mainly due to a truncation artifact, which will be discussed later.

The qM_2 distribution within the whole sample, and correspondingly the cross-link density distribution, can be displayed in the form of a histogram analysis (Figure 4a). The three maxima correspond to the average values of qM_2 of the single rubber pieces. They are well separated from each other, so that, from the width of each of the peaks, the distribution of the qM_2 values within the single pieces can be estimated. This parameter gives a measure of the cross-link density inhomogeneity in the single rubber pieces. It seems that the sample with the highest cross-link density is also the most inhomogeneous one or that at least the inhomogeneity reaches the size of the voxel and is not averaged out within the voxel volume. Figure 4b shows the corresponding T_2 histogram for this sample.

Figures 5a,b and 6a,b show the evaluations for the filled rubber sample. The results are qualitatively the same; only the range of variation of the parameters is smaller for this sample than for the unfilled sample. As a consequence, the maximum of qM_2, which corresponds to the piece of rubber with the highest cross-link density, is no more distinguishable in Figure 6a, since it is covered partially by the neighboring maximum. The shift of T_2 to lower values in Figure 6b compared with Figure 4b is typical for filled samples and corresponds to a decrease of the segmental motion under the influence of the filler.

The results of the imaging experiments qualitatively agree with the known values obtained by spectroscopic measurements of the same samples. The dependency of the T_2 values on the cross-link density is stronger and that of the qM_2 is weaker than in the spectroscopic measurements due to the zero level problem as discussed in Figure 2. For quantitative evaluation, this problem has to be solved either by elimination of the artifacts in the profiles, by improvement of the back-projection implementation, or by application of Fourier imaging. In the latter case extremely fast switching gradients have to be applied to acquire also the fast-decaying components of the transverse relaxation. If an absolute quantification is required, expression (8), which was used here for data analysis, has to be replaced for formula (6).

Another problem arises from the need to use very short τ values, since in this case the acquisition of the beginning part of the echo is not possible. As a consequence, the images will contain typical truncation artifacts. Such artifacts can be avoided, if only the decaying part of the

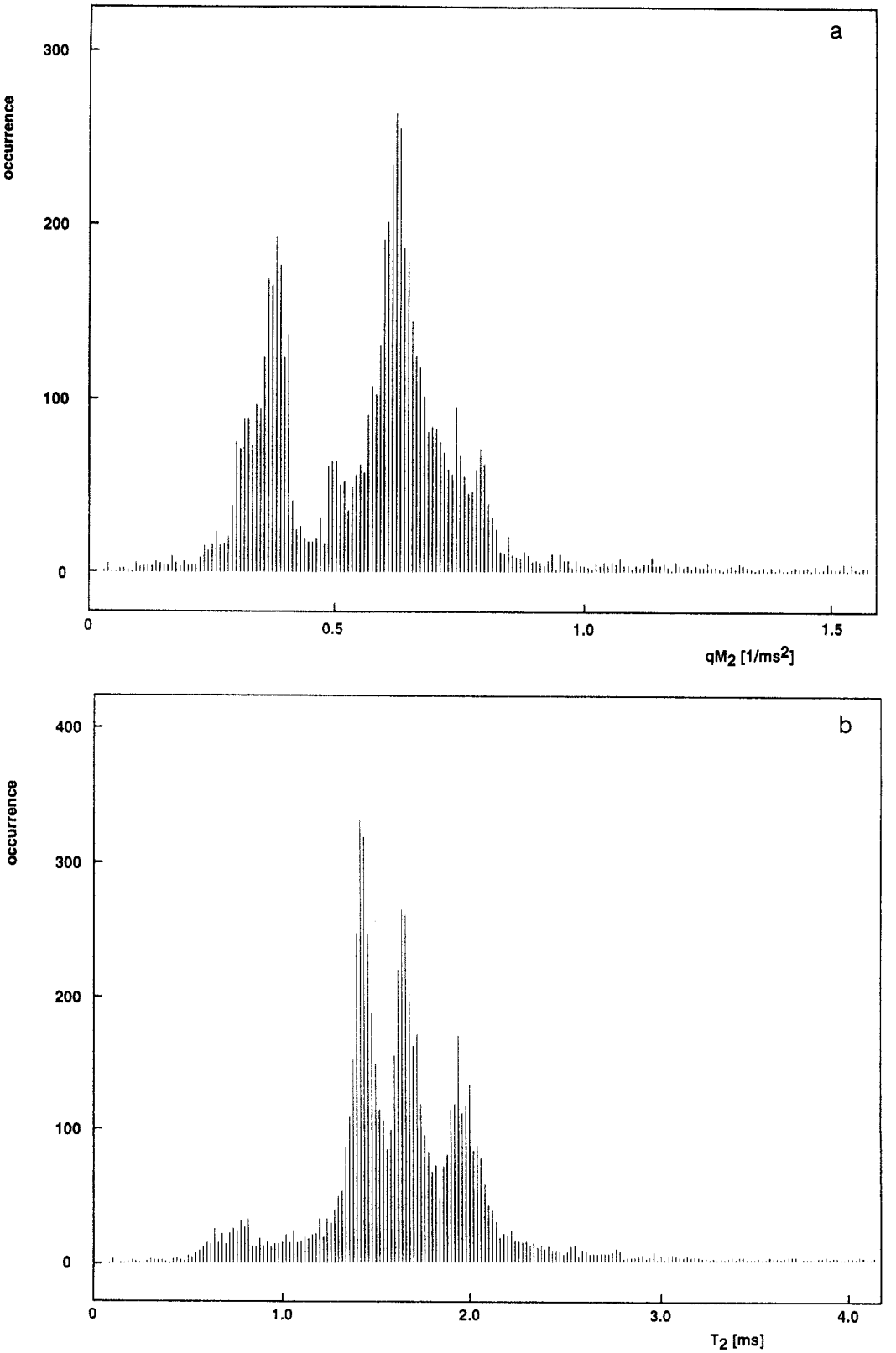

Figure 6. (a) Histogram analysis of the qM_2 distribution in the filled sample which gives qualitatively the same result as the analysis for the sample without filler (compare Figure 4a). However, the maximum corresponding to the piece of rubber with the highest cross-link density now is covered by the neighboring peak. (b) Histogram analysis of T_2 for the filled sample. Compared with Figure 4b, the range of the T_2 values is more narrow and shifted to lower values.

echo is acquired. In that case, the dispersion part will lead to an artificial broadening of the profiles. However, this problem can be overcome by proper data processing.

Conclusions

The results of the MAterial Property (MAP) imaging experiments show quite clear the potential of parameter-selective NMR imaging for the investigation of polymer networks. Interpretation of NMR data in terms of material parameters, based on a physical theory describing the molecular motion in polymers, reveals the spatial distribution of material properties. In our opinion, the transformation of NMR parameters to material properties is the key for the acceptance of NMR spectroscopy as well

as NMR imaging in materials research. In many cases the theory may be very difficult or even not developed yet, but fortunately, in the case of technical rubbers, the theory of NMR relaxation on the basis of molecular motion is well developed and its validity is proven already by spectroscopic investigations. Application to imaging is a small but important step, since not only the material parameters but also their spatial variation and distribution can be investigated.

The imaging experiment, however, introduces some problems. Besides hardware problems, which may cause some artifacts in the images and difficulties in the measurement of the fast-decaying component, the data evaluation is a problem. The multiparameter fitting procedure has to be extremely stable, since not every fit can be controlled by eye, as is possible for single spectroscopic measurements. Furthermore, it requires a minimum number of differently weighted images leading to time-consuming data acquisition and evaluation. The errors in the fit parameters and their statistical significance have to be examined in detail for more quantitative evaluation. A project dealing with these problems in connection with image analysis is currently in progress. Nevertheless, the application of NMR imaging techniques to the spatially resolved determination of material parameters relating directly to cross-link density, inter-cross-link chain mass, cross-link density inhomogeneities, and correlation times of molecular motions was performed successfully. Aging processes caused by oxidative thermal, or mechanical treatment, which may alter the cross-link density,[5] as well as imperfect curing procedures, which may result in cross-link density inhomogeneities, can be studied by this technique and will show the spatially resolved distribution of these parameters.

The idea of MAP imaging outlined above is quite general. Other materials besides polymers may be investigated in a similar way using other NMR parameters and other theoretical models. We are convinced that MAterial Property imaging as proposed above forms the bridge between NMR spectroscopists and material scientists.

Acknowledgment. Financial support by the Deutsche Forschungsgemeinschaft and the Ministère de l'Education Nationale de Luxembourg is gratefully acknowledged. The authors thank Dr. Wolff and Dr. Freund from Degussa AG for the preparation of the vulcanizates and Prof. Dr. Gronski from University of Freiburg for helpful discussions.

References and Notes

(1) Chang, C.; Komorowski, R. A. *Macromolecules* **1989**, *22*, 600.
(2) Clough, R. S.; Koenig, J. L. *Polym. Sci. Lett.* **1989**, *27*, 451.
(3) Webb, A. G.; Jezzard, P.; Hall, L. D.; Ng, S. *Polym. Commun.* **1989**, *30*, 363.
(4) Blümler, P.; Blümich, B. *Macromolecules* **1991**, *24*, 2183.
(5) Kuhn, W.; Theis, I.; Köller, E. *Adv. Tomogr. Imag. Meth. Anal. Mater., Mater. Res. Soc. Symp. Proc.* **1991**, *217*, 33.
(6) Blümich, B., Kuhn, W., Eds. *Magnetic Resonance Microscopy*; VCH: Weinheim, Germany, 1992.
(7) Blümler, P.; Blümich, B. *Acta Polym.* **1993**, *44*, 125.
(8) Smith, S. R.; Koenig, J. L. *Macromolecules* **1991**, *24*, 3496.
(9) Fedotov, V. D.; Tshernov, V. M.; Khasanovitsh, T. N. *Vysokomol. Soedin, A* **1978**, XX, *4*, 919. (The english version of the journal is *Polym. Sci. USSR.*)
(10) Gronski, W.; Hoffmann, U.; Simon, G.; Wutzler, A.; Straube, E. *Rubber Chem. Technol.* **1992**, *65*, 63.
(11) Simon, G.; Schneider, H.; Häusler, K.-G. *Prog. Colloid Polym. Sci.* **1988**, *78*, 30.
(12) Simon, G.; Götschman, B.; Matzen, D.; Schneider, H. *Polym. Bull.* **1989**, *21*, 475.
(13) Simon, G.; Baumann, K.; Gronski, W. *Macromolecules* **1992**, *25*, 3624.
(14) Kuhn, W.; Grün, F. *Kolloid Z.* **1942**, *101*, 248.
(15) Anderson, P. W.; Weiss, P. R. *Rev. Mod. Phys.* **1953**, *25*, 269.
(16) Abragam, A. *The Principles of Nuclear Magnetism*; Clarendon Press: Oxford, U.K., 1961; p 432.
(17) Bloembergen, N.; Purcell, E. M.; Pound, R. V. *Phys. Rev.* **1948**, *73*, 679.
(18) Sommer, J. U.; Heinrich, G.; Straube, E. *Colloid Polym. Sci.* **1990**, *268*, 148.
(19) Gotlib, Yu. Ya.; Lifschitz, M. J.; Shevelev, V. A.; Lishanski, J. S.; Balanina, J. V. *Vysokomol. Soedin A* **1976**, XXVIII, *10*, 2299. (The english version of the journal is *Polym. Sci. USSR.*)
(20) Staemmler, M.; Brill, R.; Becker, K.; Folkerts, K. H.; Gersonde, K. *Proceedings of the International Symposium on Comp. Ass. Radiol. CAR 89*; Springer-Verlag: Berlin, 1989.
(21) Barth, P.; Brill, R.; Staemmler, M.; Kuhn, W. In *Magnetic Resonance Microscopy*; Blümich, B., Kuhn, W., Eds.; VCH: Weinheim, Germany, 1992; p 85.